RSC Advances

PAPER

View Article Online
View Journal | View Issue

Cite this: *RSC Adv.*, 2021, **11**, 15753

Co/N-Doped hierarchical porous carbon as an efficient oxygen electrocatalyst for rechargeable Zn–air battery†

Wenshu Zhou, [a] Yanyan Liu, [a] Huan Liu,[c] Dichao Wu, [a] Gaoyue Zhang[a] and Jianchun Jiang*[ab]

Received 2nd March 2021
Accepted 12th April 2021

DOI: 10.1039/d1ra01639c

rsc.li/rsc-advances

Developing efficient electrocatalysts for ORR/OER is the key issue for the large-scale application of rechargeable Zn–air batteries. The design of Co and N co-doped carbon matrices has become a promising strategy for the fabrication of bi-functional electrocatalysts. Herein, the surface-oxidized Co nanoparticles (NPs) encapsulated into N-doped hierarchically porous carbon materials (Co/NHPC) are designed as ORR/OER catalysts for rechargeable Zn–air batteries *via* dual-templating strategy and pyrolysis process containing Co^{2+}. The fabricated electrocatalyst displays a core–shell structure with the surface-oxidized Co nanoparticles anchored on hierarchically porous carbon sheets. The carbon shells prevent Co NP cores from aggregating, ensuring excellent electrocatalytic properties for ORR with a half-wave potential of 0.82 V and a moderate OER performance. Notably, the obtained Co/NHPC as a cathode was further assembled in a zinc–air battery that delivered an open-circuit potential of 1.50 V, even superior to that of Pt/C (1.46 V *vs.* RHE), a low charge–discharge voltage gap, and long cycle life. All these results demonstrate that this study provides a simple, scalable, and efficient approach to fabricate cost-effective high-performance ORR/OER catalysts for rechargeable Zn–air batteries.

Introduction

As a promising competitor to the widely used lithium-ion battery, rechargeable Zn–air batteries have aroused tremendous interest due to their high energy density, low price, and good safety.[1–3] Its practical use is hindered by the lack of effective bifunctional electrocatalysts during discharging (oxygen reduction reaction, ORR) and charging (oxygen evolution reaction, OER).[4–6] To date, noble metal-based materials, such as Pt, RuO_2, IrO_2 and their derivatives, are commonly acknowledged as the benchmark for oxygen electrocatalysts.[7,8] Nevertheless, their high cost, scarcity, and insufficient bifunctional activity make them unattractive for large-scale applications.[9–11] Therefore, it is highly desirable to explore environmentally-friendly and effective non-noble metal electrocatalysts with more feasible fabrication strategies toward ORR and OER for rechargeable Zn–air batteries.

Recently, a number of experimental and theoretical researches have demonstrated that heteroatom (such as N, B, P, and S)-doped carbon revealed excellent electrocatalytic ORR performance with superior stability.[12–16] The origin of activity is mainly attributed to the replacement of some carbon atoms in the sp^2 lattice of graphitic carbon by heteroatoms. Then, the changed electronic arrangement of carbon-based materials tailors their electron donor properties, which are responsible for the abundant favorable active sites for electrochemical reactions.[17–19] Additionally, the introduction of transition metals, especially Fe, Co, and Ni in N-doped carbon is an effective way to produce catalysts with improved electrocatalytic performance due to the optimized electronic structure of carbon framework.[20–25] When transition metals are introduced into the carbon lattice, the electrocatalytic active sites may be produced due to the coordination function of metal atoms with the surrounding moieties.[26,27] In addition, N can bond with the metal atoms forcefully, leading to metal-like characters, and enhanced conductivities and stabilities, which synergistically enhance ORR and OER catalytic activities.[28,29] It was proposed that the density of states of Co–N across the Fermi level demonstrated by density functional theory calculation and the metallic structures of Co–N facilitate efficient electrons for effective electrocatalysis.[30,31] The modification of Co often

[a]*Institute of Chemical Industry of Forest Products, Chinese Academy of Forestry (CAF), National Engineering Lab for Biomass Chemical Utilization, Key and Open Lab. of Forest Chemical Engineering, SFA, Nanjing, Jiangsu Province, 210042, China. E-mail: jiangjc@icifp.cn*

[b]*Co-Innovation Center of Efficient Processing and Utilization of Forest Resources, Nanjing Forestry University, Nanjing, China*

[c]*College of Chemistry and Molecular Engineering, Zhengzhou University, Zhengzhou, China*

† Optimized structures of the ppC species $CBe_5H_n^{n-4}$ (n = 2–5), the results of ELF analysis for **2A–5A**, optimized structures and the relative energies of **1A–5A** and their four lowest isomers, the five independent 20 ps BOMD simulations of **2A–5A** at 500 K, the energy profile for the generation of **4C** from **4A**, and Cartesian coordinates for the species reported in this work.

happens by a surface-oxidation process to produce hydroxyl oxide species, which provide catalytic active sites for OER.[32,33] The N-doped porous carbon sheets can adsorb and transform O_2 molecules to promote ORR.[34–36] The design of Co and N co-doped carbon matrices has become a promising strategy for the fabrication of bi-functional electrocatalysts.

Carbon materials possessing hierarchical pores are beneficial to mass transport and offer a large surface area to assure sufficient exposed active sites. Thus, excellent electrochemical properties can be expected for novel hierarchically porous carbon materials. Templating methods are an important way to prepare high-quality hierarchically porous carbon materials.[37,38] Most of the approaches make use of complex templates and specific organic precursors, being unsuitable for the facile preparation of heteroatom-doped carbon materials with hierarchical pores. It is promising to develop a universal approach to produce hierarchically porous heteroatom-doped carbon by using simple templates and low-cost sustainable precursors. As a "protagonist" of industrial poverty alleviation with wide resources, low prices, and fast growth, *Broussonetia papyrifera* is attentively used in medicine, papermaking, feed processing, and other applications. To the best of our knowledge, the exploration of carbon materials derived from *Broussonetia papyrifera* for ORR/OER electrocatalysts was rarely considered.

In this work, the surface-oxidized Co nanoparticles (NPs) incorporated N-doped hierarchical porous carbon materials (Co/NHPC) are designed as ORR/OER catalysts for rechargeable Zn–air batteries. The Co/NHPC is prepared by using wood of *Broussonetia papyrifera* as a raw material *via* a dual-templating strategy, and pyrolysis process containing Co^{2+}. $Mg_5(OH)_2(CO_3)_4$ and $ZnCl_2$ were used as hard templates to obtain hierarchically porous carbon. Co/NHPC displayed core–shell structures with the surface-oxidized Co anchoring on carbon sheets. The proposed Co/NHPC-800 displays excellent ORR catalytic activity with an onset potential of 0.92 V and a tiny 10 mV loss in half-wave potential ($E_{1/2}$) after 10 000 cycles. The rechargeable Zn–air batteries based on Co/NHPC-800 reveal a low charge–discharge voltage gap that remained nearly unchanged after 1092 cycles (about 364 h) at 5 mA cm^{-2}. The excellent performance may be attributed to: (i) the hierarchical pores of carbon material offering a mass transport and large surface area to assure sufficient exposed active sites; (ii) carbon shells can prevent Co NPs cores from aggregating, ensuring excellent catalytic stability;[39] (iii) the surface-oxidized Co NPs cores providing catalytic active sites for OER, and the N-doped porous carbon sheets are beneficial to promoting ORR. To sum up, this study offers a promising way to prepare a cost-effective and high-efficient ORR/OER catalysts for rechargeable metal–air batteries.

Experimental section

Synthesis of NHPC

The branches of *Broussonetia papyrifera* were cut into small pieces and washed with ethanol and distilled water successively, then dried in a vacuum at 80 °C for 24 h. Then, they were ground into powder and sieved using a 100-micron mesh. The powder (20 g) was dissolved in H_3BO_3 solution (2 M) and subjected to a hydrothermal reaction at 180 °C for 30 h to obtain hydrothermal carbon. The hydrothermal carbon (1 g), $Mg_5(OH)_2(CO_3)_4$ (1 g), $ZnCl_2$ (3 g) and urea (0.54 g) were ground with a ball mill for 30 min, then the mixture was calcinated at 900 °C for 2 h with a ramp rate of 5 °C·min^{-1} under N_2. The obtained material was immersed in HCl solution (2 M) for 24 h, washed with water several times, and dried at 60 °C overnight. The hierarchically porous nitrogen-doped carbon (NHPC) was produced. Without adding urea, hierarchically porous carbon (HPC) was synthesized *via* the similar procedure of NHPC.

Synthesis of Co/NHPC-T

NHPC (200 mg) and cobalt(II)acetylacetonate (1 mmol) were added to ethanol (200 mL). After being continuously stirred for 12 h at room temperature, the mixture was obtained by filtration and dried at 60 °C for 12 h in a vacuum desiccator. Cobalt(II)acetylacetonate–NHPC was pyrolyzed at the desired temperature (700, 800 and 900 °C) for 2 h with a rate of 5 °C min^{-1} under N_2. The cobalt incorporated in N-doped hierarchically porous carbon was obtained and denoted as Co/NHPC-T.

Characterization

The microstructure of the as-prepared products was characterized by transmission electron microscopy (TEM, JEOL-JEM-2100, operating at 200 kV), and scanning electron microscopy (SEM, JEOL JSM 7800F) with elemental mappings collected by EDAX. The crystalline phase structures of products were analyzed using X-ray diffraction (XRD, Bruker D8 advance with Cu Kα, λ = 1.5418 Å). Raman spectra were recorded on a Renishaw RM-1000 with Ar-ion laser (λ = 514 nm, power = 8.0 mw). The surface compositions of the samples were analyzed using X-ray photoelectron spectroscopy (XPS) on the Thermo Scientific K-Alpha+ with Al Kα X-ray as the excitation source. N_2 sorption isotherms were performed at 77.35 K on a Micromeritics Tristar 3020 surface area and porosity analyzer after the sample was degassed in a vacuum at 200 °C for 4 h.

Electrochemical measurements

ORR/OER measurements were carried out in a three-electrode system connected to an electrochemical analyzer (CHI 760E), coupled with a rotating ring-disk electrode (RRDE) system (Pine Instruments Co. Ltd, USA) at room temperature. An Ag/AgCl electrode was used as the reference electrode. The counter electrodes for ORR and OER were a platinum wire and a graphite rod, respectively. All the measured potentials were converted to a reversible hydrogen electrode (RHE) by the following equation:

$$E\,(vs.\ \mathrm{RHE}) = E\,(vs.\ \mathrm{Ag/AgCl}) + 0.197 + 0.059\mathrm{pH} \quad (1)$$

The electrocatalyst (4 mg) was dispersed ultrasonically for 60 min in a mixed solvent containing ethanol (720 μL) and Nafion (0.5 wt%, 80 μL). Then, 10 μL of the dispersion was cast on a polished glassy carbon electrode (5 mm diameter) and allowed to dry at room temperature. The glassy carbon

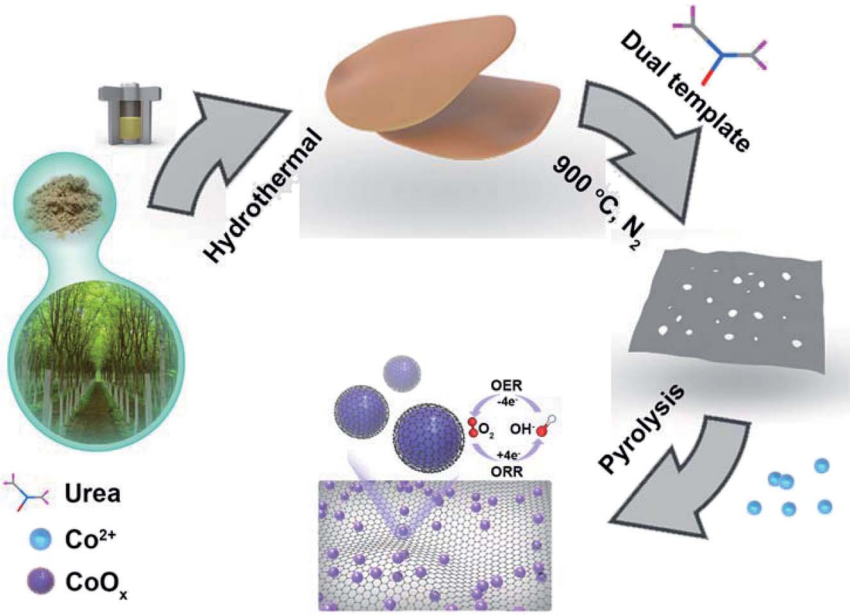

Fig. 1 Schematic synthesis procedures of Co/NHPC-T.

electrodes well-proportionately coated with samples (loading of the electrocatalyst amount was ~0.254 mg cm^{-2}) were used as the working electrode. The linear sweep voltammetry (LSV) was conducted in 0.1 M KOH solution for ORR and OER with a scan rate of 5 mV s^{-1}. The presented current density was normalized to the geometric surface area of electrodes. The poison tests for

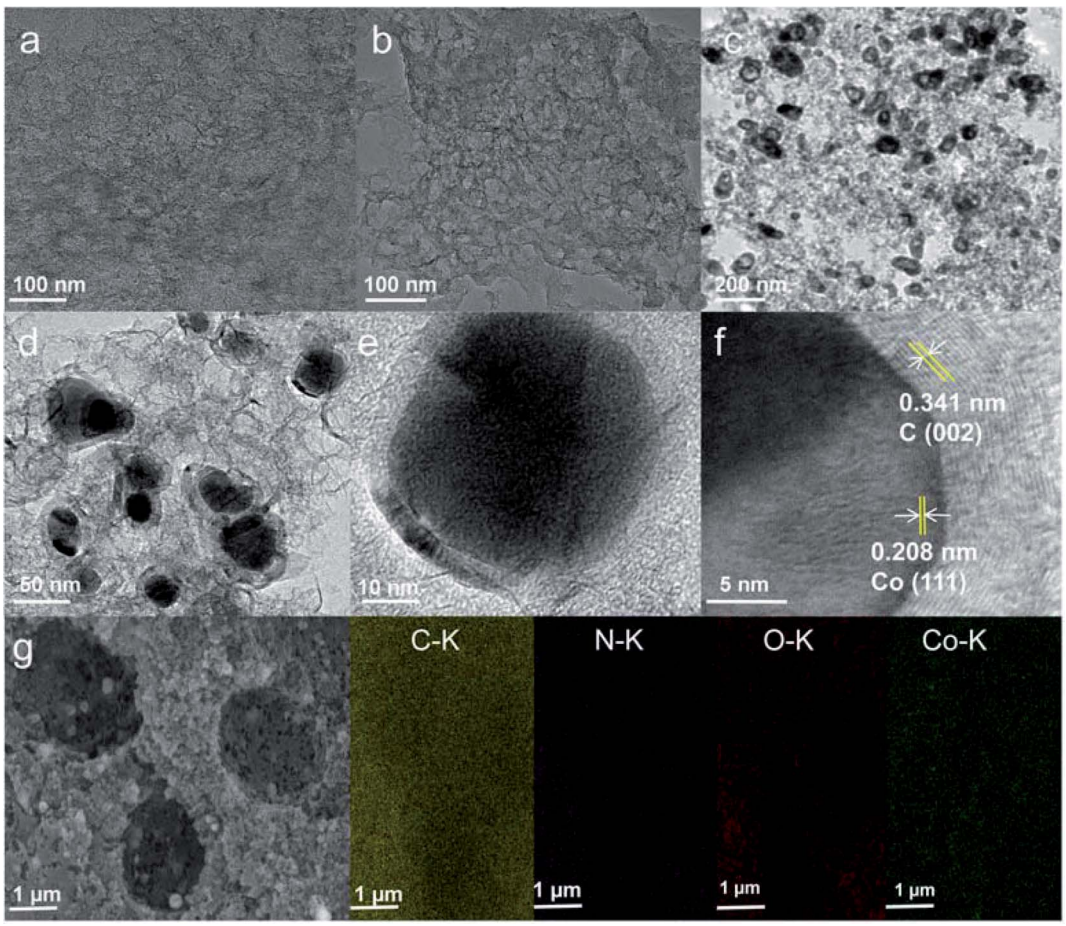

Fig. 2 TEM images of (a) HPC, (b) NHPC, (c–f) Co/NHPC-800, and (g) SEM image and the corresponding EDX elemental mapping images of Co/NHPC-800.

ORR were performed in mixed solutions containing KOH (0.1 M) and CH_3OH (1 M). Rotating ring disk electrode (RRDE) measurements were carried out in O_2-saturated KOH (0.1 M) at 1600 rpm at a scan rate of 5 mV s^{-1}, and the potential of the Pt ring was set at 1.3 V (*vs.* RHE). The electron transfer number (n) and the yield of hydrogen peroxide released during ORR was calculated through the following equation:

$$n = 4 \times \frac{I_D}{I_D + I_R/N} \quad (2)$$

$$[H_2O_2]\% = 200 \times \frac{I_R/N}{I_R/N + I_D} \quad (3)$$

where I_D is the disk current, I_R is the ring current, and N is the collection coefficient of the Pt ring ($N = 0.37$). Furthermore, commercial Pt/C electrocatalysts were used as a reference to evaluate the electrocatalytic performance of various samples.

RZABs were assembled with catalyst-coated carbon paper as the air cathode, a polished Zn plate as the anode, and KOH (6.0 M) containing zinc acetate (0.2 M) aqueous solution as the electrolyte. The mass of the catalyst loading was 1 mg cm^{-2}. Disposing the gas dispersion film (GDL) on the positive

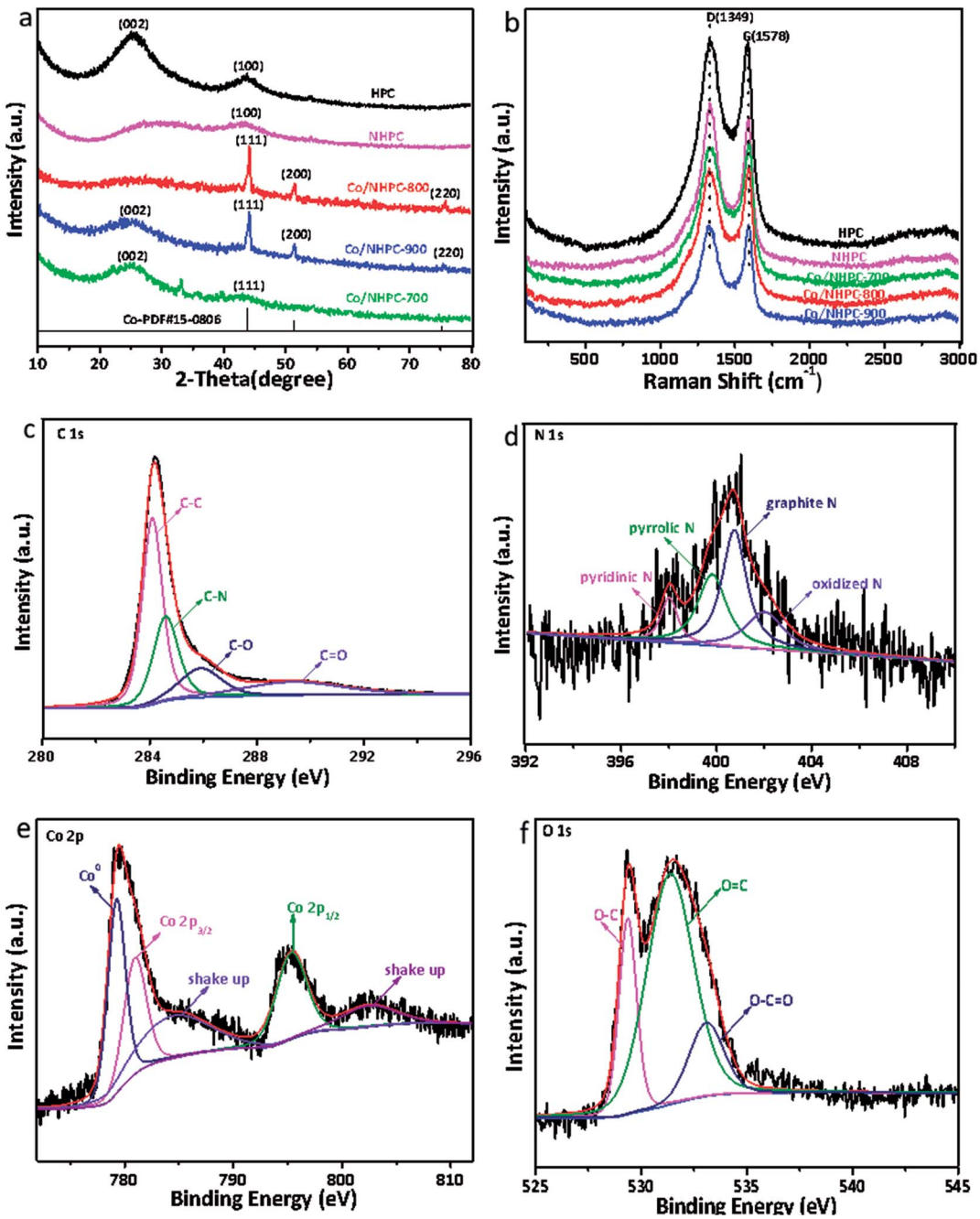

Fig. 3 (a) XRD patterns (b) Raman spectra of HPC, NHPC, Co/NHPC-700, Co/NHPC-800, Co/NHPC-900, (c) C 1s spectrum, (d) N 1s spectrum, (e) Co 2p spectrum, and (f) O 1s spectrum of Co/NHPC-800.

electrode so that the gas can be well transferred to the cathode. Celgard 2340 microfiber filter was utilized as a separator. The discharge/charge cycling of RZABs was conducted using an automatic battery testing system (Neware CT-3008) with 20 min for each cycle (discharge 10 min; charge 10 min) at 5 mA cm^{-2}. Polarization data (v–i) were collected using linear sweep voltammetry (LSV) at a scan rate of 10 mV s^{-1}. The current and power density curves were calculated from LSV curves. All tests were performed in a natural environment.

Results and discussion

The fabrication process of Co/NHPC-T is schematically described in Fig. 1. First, the raw material was subjected to a hydrothermal reaction. Then, the hydrothermal carbon mixed with $Mg_5(OH)_2(CO_3)_4$, $ZnCl_2$ and urea were pyrolyzed in N_2 atmosphere at 900 °C, followed by etching treatment with HCl solution to obtain NHPC. During this process, $Mg_5(OH)_2(CO_3)_4$ and $ZnCl_2$ served as templates to produce hierarchically porous carbon, and urea were used as a nitrogen source. Finally, Co/NHPC-T was prepared by the pyrolysis of NHPC that was adsorbed with Co^{2+}. The morphologies of the synthesized catalysts were studied using TEM and SEM analysis. HPC and NHPC showed the characteristics of porous carbon sheets (Fig. S1a, b† and 2a, b). Images of Co/NHPC-800 confirmed that the uniform Co NPs were anchored onto the porous carbon sheets (Fig. 2c and d). The representative HRTEM image exhibited the existence of Co NPs and the surrounding carbon layers (Fig. 2e). The lattice fringes with interplanar spacings of 0.341 and 0.208 nm could be observed, which corresponded to (022) planes of graphite C and (111) planes of metallic Co, respectively (Fig. 2f). The EDX elemental mapping images revealed the uniform distribution of C, Co, N, and O in Co/NHPC-800 (Fig. 2g). The O element indicated the generation of surface-oxidized Co NPs which are beneficial to promote OER. Co/NHPC-700 and Co/NHPC-900 showed morphology similar to that of Co/NHPC-800 (Fig. S1c and f†), but their Co NPs were larger and randomly distributed on the carbon sheets (Fig. S1e and f†).

The chemical compositions of the as-made catalysts were researched *via* XRD (Fig. 3a). The XRD patterns of HPC and NHPC showed two broadened peaks at 24.5° and 43.5°, which are assigned to (002) and (101) diffraction peaks of carbon,[40] respectively. In addition to carbon peaks, Co/NHPC-T showed peaks of cobalt species. The peaks at 44.3°, 51.6° and 75.8° in Co/NHPC-800 and Co/NHPC-900 are attributed to the (111), (200), and (220) lattice facets of metallic cubic-phase Co, respectively.[41] Co/NHPC-700 displays peaks at 32.1°, assigned to lattice facets of cobalt oxide.[42] Raman spectra of the as-prepared catalysts are depicted in Fig. 3b, and the samples reveal similar peaks. The D bands at 1349 cm^{-1} are due to the disordered carbon, and the G bands at 1578 cm^{-1} are ascribed to the sp^2 graphitic carbon.[43] The I_D/I_G values of HPC, NHC, Co/NHPC-700, Co/NHPC-800 and Co/NHPC-900 are 1.04, 1.01, 1.03, 1.02 and 1.03, respectively. All the samples possess similar and relatively high I_D/I_G, confirming more disordered carbon in their framework. The surface chemical composition and valence state of the Co/NPHC-800 catalyst was identified by XPS. The full spectrum clearly reveals the copresence of C, N, O and Co elements with atomic percentages of 92.8%, 1.15%, 4.9% and 1.16%, respectively (Fig. S2 and Table S1†). The C 1s spectrum displays four peaks at around 284.1 eV, 285.1 eV, 286.0 eV and 287.2 eV, which are corresponding to the carbon states of C=C/C–C, C–O/C=N, C=O/C–N and O=C–O bonds, respectively[44] (Fig. 3c). The high-resolution spectrum of N 1s shows the presence of four types of nitrogen species, attributed to pyridinic N at 398.0 eV, pyrrolic N at 399.8 eV, graphite N at 400.7 eV and oxidized N at 402.0 eV (ref. 45 and [46]) (Fig. 3d). The

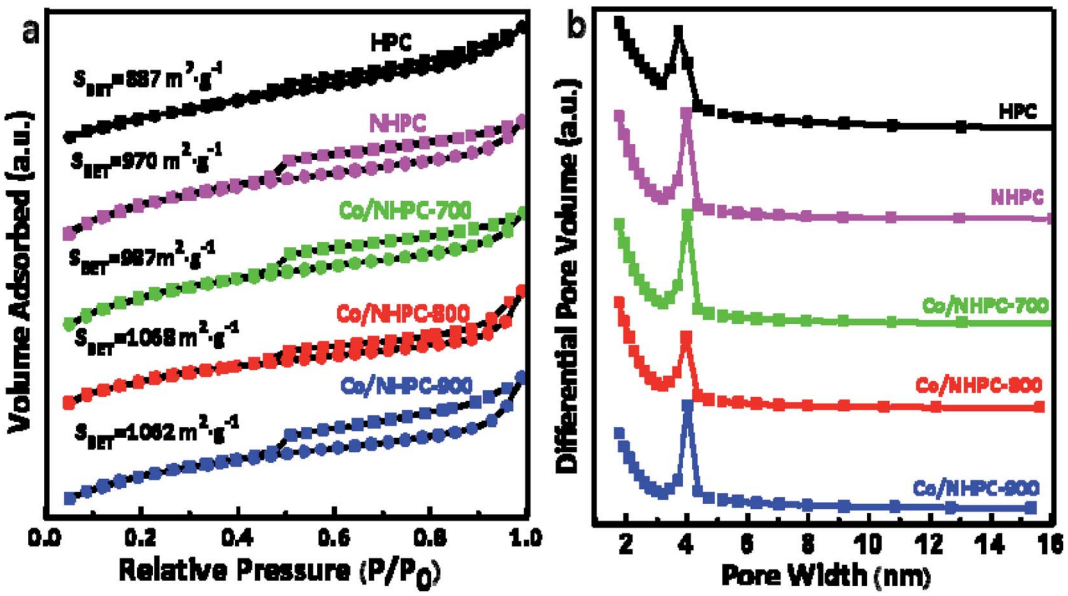

Fig. 4 (a) Nitrogen adsorption–desorption isotherms and (b) pore size distributions of HPC, NHPC, Co/NHPC-700, Co/NHPC-800 and Co/NHPC-900.

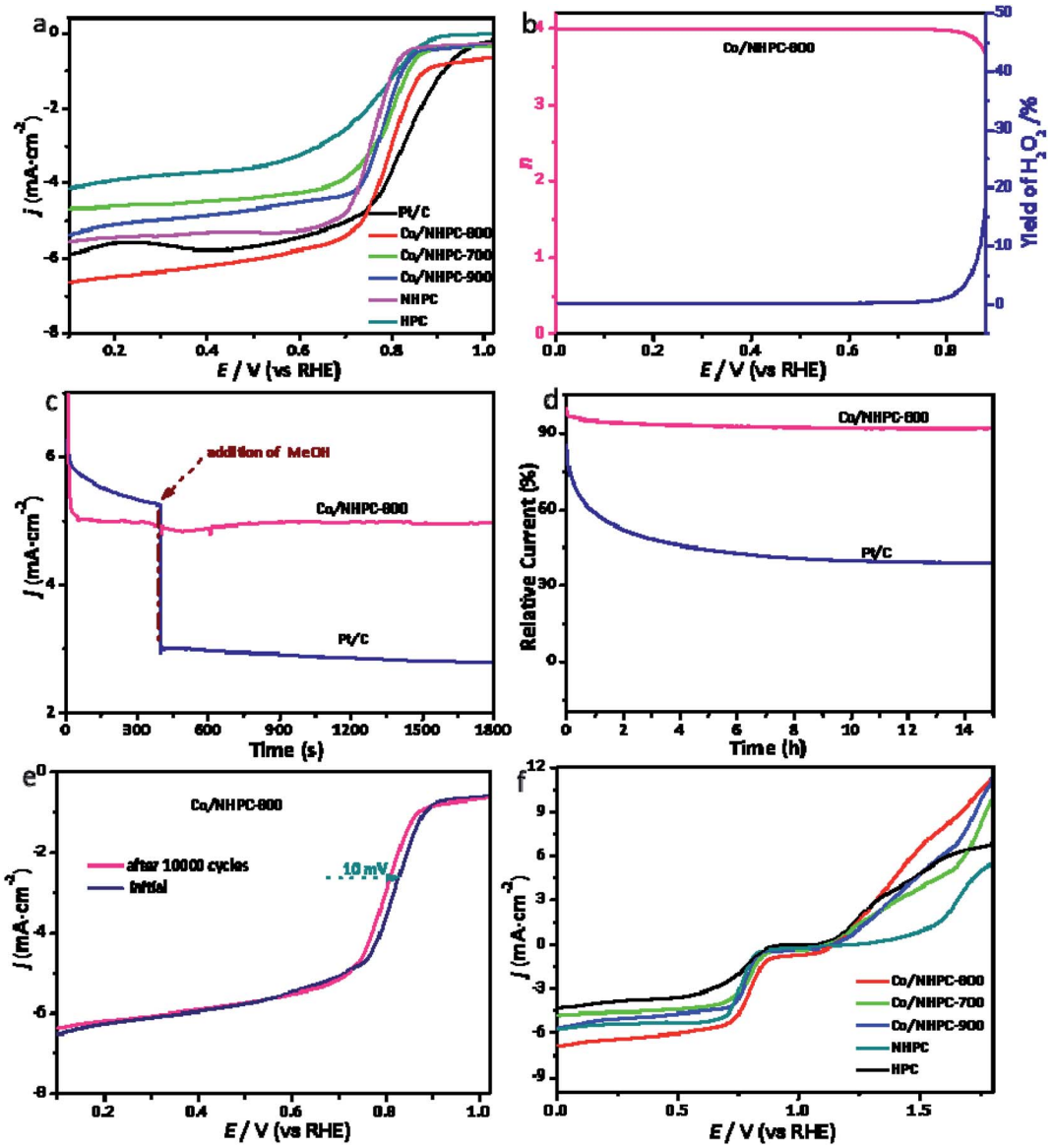

Fig. 5 (a) LSV curves of HPC, NHPC, Co/NHPC-700, Co/NHPC-800, Co/NHPC-900 and Pt/C at 1600 rpm with 5 mV s^{-1}, (b) the electron transfer number (*n*) and peroxide yield of Co/NHPC-800 at 1600 rpm, (c) methanol tolerance tests of Co/NHPC-800 with methanol (1 M), (d) chronoamperometry curves of Co/NHPC-800 and Pt/C electrodes at 0.4 V (*vs.* RHE) at 1800 rpm, (e) accelerated durability test (ADT) of Co/NHPC-800, and (f) LSV curves of HPC, NHPC, Co/NHPC-700, Co/NHPC-800 and Co/NHPC-900 at 1800 rpm, showing the electrocatalytic activities for ORR and OER.

peak around 779.1 eV is assigned to Co^0 species.[47] The peak at 781.1 eV corresponds to Co^{2+}, and the peak at 795.6 eV is ascribed to Co $2p_{1/2}$.[48] The appearance of Co^{2+} species proves the generation of surface-oxidized Co NPs which are conducive to improving the electrocatalytic activity. The peaks at 785.7 and 803.1 eV are shake-up satellite peaks[49] (Fig. 3e). The O1s spectrum can be fitted into three peaks at 529.0 eV, 530.8 eV and 533.0 eV, which correspond to O–C, O=C and O–C=O, respectively[50] (Fig. 3f).

The porosity of the as-made catalysts was further investigated through N_2 adsorption–desorption studies. The classical H4-type hysteresis loops in isotherms present the characteristics of mesoporous structures.[51] The greatly increasing adsorption capacities in the low P/P_0 indicate the existence of micropores.[52] The surface areas of HPC, NHPC, Co/NHPC-700, Co/NHPC-800, and Co/NHPC-900 are 887 $m^2\ g^{-1}$, 971 $m^2\ g^{-1}$, 987 $m^2\ g^{-1}$, 1068.1 $m^2\ g^{-1}$ and 1061 $m^2\ g^{-1}$, respectively, while the pore volumes of HPC, NHPC, Co/NHPC-700, Co/NHPC-800 and Co/NHPC-900 are 0.59 $cm^3\ g^{-1}$, 0.43 $cm^3\ g^{-1}$, 0.50 $cm^3\ g^{-1}$, 0.57 $cm^3\ g^{-1}$ and 0.64 $cm^3\ g^{-1}$, respectively (Table S2†). The hierarchical porosity of carbon samples is beneficial to expose catalytic active sites and promote the diffusion of ions during the electrocatalytic ORR/OER process. The macropores and large mesopores can work as solution buffering reservoirs to minimize the diffusion distance to the mesopores (or micropores) and facilitate mass transport. The high efficient mass

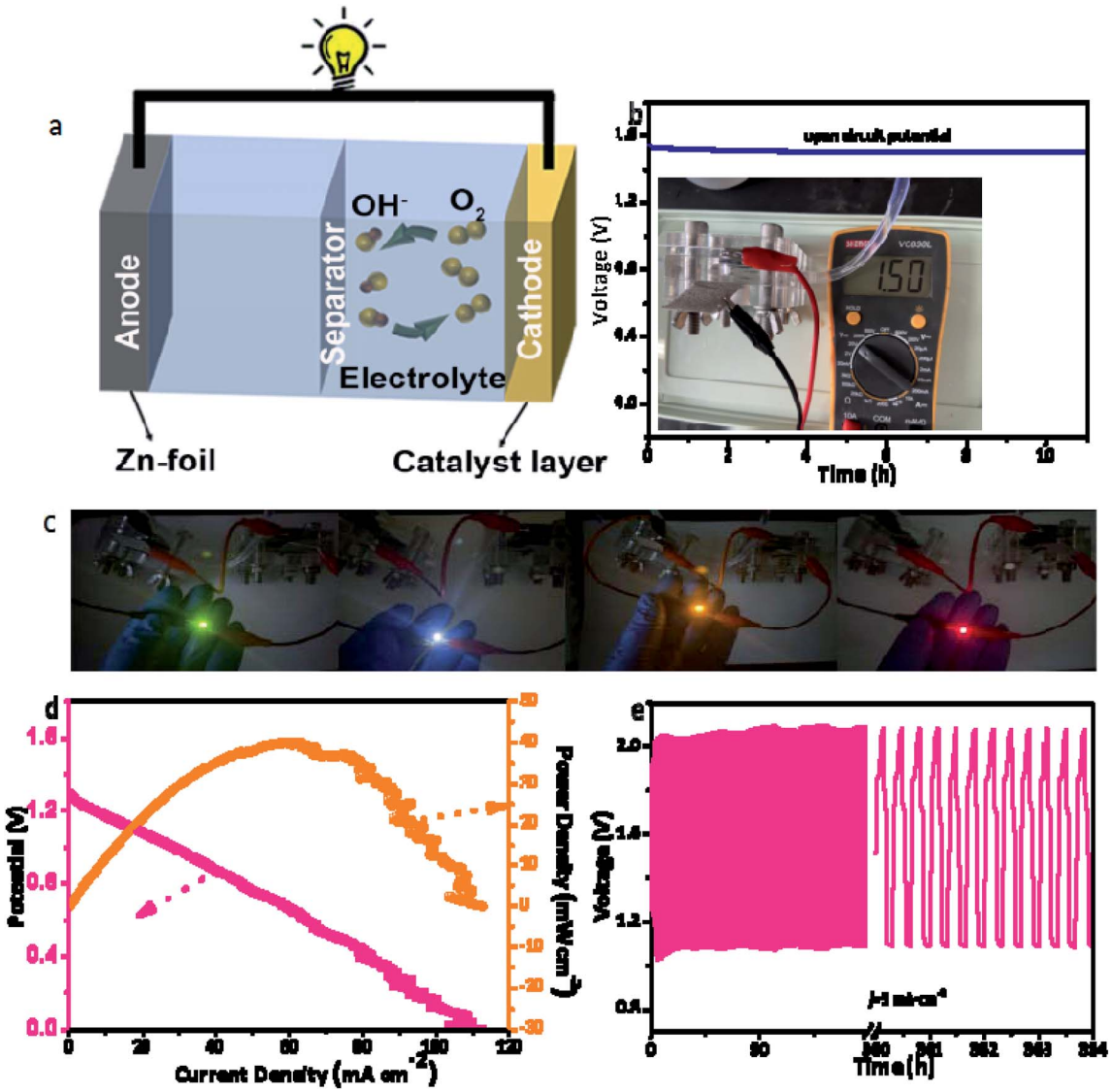

Fig. 6 (a) A simple illustration of ZABs, (b) the open-circuit plots of a single battery, (c) blue, red, yellow and green LEDs powered by two-series batteries based on Co/NHPC-800, (d) discharge polarization curves and corresponding power density of ZABs based on Co/NHPC-800 and Pt/C, and (e) long-term cycling stability of RZABs based on Co/NHPC-800.

diffusion helps the catalytically active sites work well for ORR–OER conversion. The volume change during the charge/discharge cycling is reduced to ensure a high cycling performance (Fig. 4).[53–58]

The electrocatalytic performance of catalysts for ORR were evaluated in 0.1 M KOH solution. Cycle voltammetry (CV) tests were firstly measured in N_2/O_2-saturated solution (Fig. S3†). All electrocatalysts show obvious cathodic ORR peaks in O_2-saturated KOH solution, but no peak in N_2-saturated KOH solution. The more positive peak for ORR of Co/NHPC-800 than that for WC, HPC, NHPC, Co/NHPC-700 and Co/NHPC-900, states its excellent ORR electrocatalytic activity. The ORR polarization curves of these catalysts in Fig. 5a further demonstrate the superior electroactivity of Co/NHPC-800. Co/NHPC-800 exhibits excellent ORR electrocatalytic activity with a high half-wave potential ($E_{1/2}$) of 0.82 V. This value is a little negative than that of Pt/C (0.84 V), and more positive than those for WC (0.62 V), HPC (0.76 V), NHPC (0.77 V), Co/NHPC-700 (0.79 V), Co/NHPC-900 (0.78 V). The $E_{1/2}$ value of Co/NHPC-800 is superior to many other available non-noble metal catalysts (Table S3†). Fig. S4† shows ORR polarization curves of Co/NHPC-800 at different rotating rates. Co/NHPC-800 shows incremental limiting current density with the increase of rotational speed due to overcoming the diffusion limitation. RRDE tests were carried out to research H_2O_2 production during the ORR process of Co/NHPC-800. The electron transfer number (n) of ORR was 3.89–3.99 per oxygen molecule from 0.2 V to 0.85 V. The corresponding H_2O_2 yield was generally below 3.2 mol% (Fig. 5b). These results reveal a dominant $4e^-$ a reduction pathway in the ORR process. The measurements of tolerance to methanol were also conducted for Co/NHPC-800 and Pt/C. After the addition of methanol into the electrolyte, the current

density of Pt/C drops drastically. Whereas it shows no obvious change for Co/NHPC-800, indicating its excellent tolerance to methanol crossover effect (Fig. 5c). Fig. 5d shows results on the chronoamperometry test of Co/NHPC-800 and Pt/C conducted at 0.40 V (*vs.* RHE) for 15 h. At the end of the test, Co/NHPC-800 maintained 92.14% of its initial current density, demonstrating its good stability for ORR. In addition, the accelerated degradation test (ADT) was conducted *via* continuous CV tests between 0.20 and 1.05 V (*vs.* RHE) for 10 000 cycles at 100 mV s^{-1}. As described in Fig. 5e, after the ADT test, the $E_{1/2}$ of Co/NHPC-800 shifts without clear deviation (about 10 mV), further illustrating its robust stability. The OER electroactivity of the as-prepared catalysts was also measured in KOH (0.1 M). Compared with HPC, NHPC, Co/NHPC-700 and Co/NHPC-900, Co/NHPC-800 exhibits a more promising OER activity (Fig. 5f). ORR, OER and dual catalytic activity of Co/NHPC-800 are comparable to some reported works in the literature (Table S3†). The dual ORR/OER electroactivities of Co/NHPC-800 reveals that it possesses the potential to apply as cathode materials in rechargeable metal–air batteries.

The outstanding bifunctional ORR/OER performance of Co/NHPC-800 inspires us to evaluate its application in practical RZABs. A homemade rechargeable Zn–air battery was assembled using Co/NHPC-800 as the air cathode, Zn plate as the anode, and 6.0 M KOH + 0.2 M $Zn(CH_3COO)_2$ as the electrolyte (Fig. S5 and S6†). The diagram of ZAB is shown in Fig. 6a, and as can be seen in Fig. 6b, RZABs based on Co/NHPC-800 displays a high open-circuit voltage (V_{OC}) of 1.5 V, confirming the good electroactivity of Co/NHPC-800. The two RZABs based on Co/NHPC-800 successfully light a 2.2 V light-emitting diode (LED) (Fig. 6c). The RZABs based on Co/NHPC-800 exhibit a maximum power density of about 40 mW cm^{-2} (Fig. 6d). The recharging ability of RZABs based on Co/NHPC-800 was measured continuously with 20 min for each step at 5 mA cm^{-2}. The charge–discharge voltage gap (1.01 V at the 1st h and 0.99 V at the 364th h) of RZABs was nearly unchanged after 1092 cycles (about 364 h) (Fig. 6e), confirming the superior electrocatalytic stability of Co/NHPC-800. The cycling performances of RZABs surpass that of the batteries reported in the literature (Table S3†). The excellent durability of the RZABs proves that Co/NHPC-800 possesses great potential for being used in energy storage devices.

Conclusions

In conclusion, surface-oxidized Co NPs encapsulated in N-doped hierarchical porous carbon materials (Co/NHPC) are designed as ORR/OER catalysts for rechargeable Zn–air batteries. The Co/NHPC displays core–shell structures with surface-oxidized Co NPs@C cores anchoring on the carbon sheets. The hierarchical porous structure of Co/NHPC enabled the material facile mass transport and offer a large surface area to assure sufficient exposed active sites, while the synergistic effect between N-doping and surface-oxidized Co NPs provided the Co/NHPC with remarkable catalytic activity. The rechargeable Zn–air batteries based on Co/NHPC-800 revealed a high open-circuit potential (1.50 V, superior to that of Pt/C), low charge–discharge voltage gap and long cycle life of nearly 1092 cycles (about 364 h) at 5 mA cm^{-2}. This work offers a promising way to prepare cost-effective, high-efficient ORR/OER catalysts for rechargeable metal–air batteries.

Conflicts of interest

The work has not been published before and is not being submitted to any other journal for publication. The authors declare that they have no conflicts of interest.

Acknowledgements

Financial support from the National Natural Science Foundation of China (no. 31901272) and the Jiangsu Province Key Laboratory of Biomass Energy and Materials (no. JSBEM-S-201906) are acknowledged.

References

1 Y. Li and H. Dai, *Chem. Soc. Rev.*, 2014, **43**, 5257–5275.
2 D. Ji, L. Fan, L. Li, S. Peng, D. Yu, G. Song, S. Ramakrishna and S. Guo, *Adv. Mater.*, 2019, **31**, 1808267.
3 G. M. Pereira, T. S. C. Cellet, A. F. Rubira and R. Silva, *ACS Appl. Energy Mater.*, 2018, **1**, 4939–4949.
4 J. Pan, Y. Xu, H. Yang, Z. Dong, H. Liu and B. Xia, *Adv. Sci.*, 2018, **5**, 1700691.
5 J. Li, Y. Zhu, W. Chen, Z. Lu, J. Xu, A. Pei, Y. Peng, X. Zheng, Z. Zhang, S. Chu and Y. Cui, *Joule*, 2019, **3**, 557–569.
6 Y. Wang, B. Fang, X. Wang, A. Ignaszak, Y. Liu, A. Li, L. Zhang and J. Zhang, *Prog. Mater. Sci.*, 2018, **98**, 108–167.
7 M. Fan, J. Cui, J. Wu, R. Vajtai, D. Sun and P. M. Ajayan, *Small*, 2020, **16**, 1906782.
8 Y. Nie, L. Li and Z. Wei, *Chem. Soc. Rev.*, 2015, **44**, 2168–2201.
9 H. Xu, B. Wang, C. Shan, P. Xi, W. Liu and Y. Tang, *ACS Appl. Mater. Interfaces*, 2018, **10**, 6336–6345.
10 X. Ma, K. Li, X. Zhang, B. Wei, H. Yang, L. Liu, M. Zhang, X. Zhang and Y. Chen, *J. Mater. Chem. A*, 2019, **7**, 14904–14915.
11 Z. Wang, D. Xu, J. Xu and X. Zhang, *Chem. Soc. Rev.*, 2014, **43**, 7746–7786.
12 D. Yu, L. Zhou, J. Tang, J. Li, J. Hu, C. Peng and H. Liu, *Ind. Eng. Chem. Res.*, 2017, **56**, 8880–8887.
13 S. Wang, X. Ji, Y. Ao and J. Yu, *ACS Appl. Mater. Interfaces*, 2018, **10**, 29866–29875.
14 Z. Wang, H. Liu, R. Ge, X. Ren, J. Ren, D. Yang, L. Zhang and X. Sun, *ACS Catal.*, 2018, **8**, 2236–2241.
15 A. El-Sawy, I. Mosa, D. Su, C. Guild, S. Khalid, R. Joesten, R. Rusling and S. Suib, *Adv. Energy Mater.*, 2016, **6**, 1501966.
16 L. Yang, S. Jiang, Y. Zhao, L. Zhu, S. Chen, X. Wang, Q. Wu, J. Ma, Y. Ma and Z. Hu, *Angew. Chem., Int. Ed.*, 2011, **50**, 7132–7135.
17 D. Guo, R. Shibuya, C. Akiba, S. Saji, T. Kondo and J. Nakamura, *Science*, 2016, **351**, 361–365.
18 J. Zhang, Z. Zhao, Z. Xia and L. Dai, *Nat. Nanotechnol.*, 2015, **10**, 444–452.

19 G. Wu, A. Santandreu, W. Kellogg, S. Gupta, O. Ogoke, H. Zhang, H. Wang and L. Dai, *Nano Energy*, 2016, **29**, 83–110.
20 Q. Wang, L. Shang, R. Shi, X. Zhang, Y. Zhao, G. Waterhouse, L. Wu, C. Tung and T. Zhang, *Adv. Energy Mater.*, 2017, **7**, 1700467.
21 J. Yin, Y. Li, F. Lv, Q. Fan, Y. Zhao, Q. Zhang, W. Wang, F. Cheng, P. Xi and S. Guo, *ACS Nano*, 2017, **11**, 2275–2283.
22 P. Thakur, M. Yeddala, K. Alam, P. Pal, P. Sen and T. N. Narayanan, *ACS Appl. Energy Mater.*, 2020, **3**, 7813–7824.
23 T. N. Tran, H. Y. Lee, J. D. Park, T. H. Kang, B. J. Lee and J. S. Yu, *ACS Appl. Energy Mater.*, 2020, **3**, 6310–6322.
24 S. Shen, Z. Lin, K. Song, Z. Wang, L. Huang, L. Yan, F. Meng, Q. Zhang, L. Gu and W. Zhong, *Angew. Chem., Int. Ed.*, 2021, DOI: 10.1002/anie.202102961.
25 Z. X. Huang, X. P. Qin, G. Z. Li, W. C. Yao, J. Liu, N. G. Wang, K. Ithisuphalap, G. Wu, M. H. Shao and Z. C. Shi, *ACS Appl. Energy Mater.*, 2019, **2**, 4428–4438.
26 S. Chao, G. Wang, D. Xu and Y. Wang, *Int. J. Hydrogen Energy*, 2018, **43**, 11012–11021.
27 M. Wu, E. Zhang, Q. Guo, Y. Wang, J. Qiao, K. Li and P. Pei, *Appl. Energy*, 2016, **175**, 468–478.
28 K. Yoon, K. Shin, J. Park, S. Cho, C. Kim, J. Jung, J. Cheong, H. Byon, H. Lee and I. Kim, *ACS Nano*, 2018, **12**, 128–139.
29 M. Fan, J. Cui, J. Zhang, J. Wu, S. Chen, L. Song, Z. Wang, A. Wang, R. Vajtai, Y. Wu, P. M. Ajayan, J. Jiang and D. Sun, *J. Mater. Sci. Technol.*, 2021, DOI: 10.1016/j.jmst.2021.01.093.
30 Z. Chen, Y. Ha, Y. Liu, H. Wang, H. Yang, H. Xu, Y. Li and R. Wu, *ACS Appl. Mater. Interfaces*, 2018, **10**, 7134–7144.
31 P. Chen, K. Xu, Z. Fang, Y. Tong, J. Wu, X. Lu, X. Peng, H. Ding, C. Wu and Y. Xie, *Angew. Chem., Int. Ed.*, 2015, **54**, 14710–14714.
32 J. Gao, N. Ma, J. Zhai, T. Li, W. Qin, T. Zhang and Z. Yin, *Ind. Eng. Chem. Res.*, 2015, **54**, 7984–7989.
33 D. Wu, C. Zhu, Y. Shi, H. Jing, J. Hu, X. Song, D. Si, S. Liang and C. Hao, *ACS Sustainable Chem. Eng.*, 2019, **7**, 1137–1145.
34 W. Yuan, Y. Feng, A. Xie, X. Zhang, F. Huang, S. Li, X. Zhang and Y. Shen, *Nanoscale*, 2016, **8**, 8704–8711.
35 D. Yu, L. Zhou, J. Tang, J. Li, J. Hu, C. Peng and H. Liu, *Ind. Eng. Chem. Res.*, 2017, **56**, 8880–8887.
36 S. Liu, C. Deng, L. Yao, H. Zhong and H. Zhang, *J. Power Sources*, 2014, **269**, 225–235.
37 Y. Wang, B. Fang, D. Zhang, A. Li, D. Wilkinson, A. Ignaszak, L. Zhang and J. Zhang, *Electrochem. Energy Rev.*, 2018, **1**, 1–34.
38 S. Dutta, A. Bhaumik and K. Wu, *Energy Environ. Sci.*, 2014, **7**, 3574–3592.
39 Y. Xing, S. Wang, B. Fang, G. Song, D. Wilkinson and S. Zhang, *J. Power Sources*, 2018, **385**, 10–17.
40 Y. Yao, C. Xu, J. Qin, F. Wei, M. Rao and S. Wang, *Ind. Eng. Chem. Res.*, 2013, **52**, 17341–17350.
41 Y. Liu, G. Han, X. Zhang, C. Xing, C. Du, H. Cao and B. Li, *Nano Res.*, 2017, **10**, 3035–3048.
42 P. Yin, T. Yao, Y. Wu, L. Zheng, Y. Lin, W. Liu, H. Ju, J. Zhu, X. Hong, Z. Deng, G. Zhou, S. Wei and Y. Li, *Angew. Chem., Int. Ed.*, 2016, **55**, 10800–10805.
43 L. Xie, G. Sun, F. Su, X. Guo, Q. Kong, X. Li, X. Huang, L. Wan, W. Song, K. Li, C. Lv and C. Chen, *J. Mater. Chem. A*, 2016, **4**, 1637–1646.
44 B. B. Huang, Y. C. Liu and Z. L. Xie, *J. Mater. Chem. A*, 2017, **5**, 23481–23488.
45 S. Zhang, K. Tian, B. Cheng and H. Jiang, *ACS Sustainable Chem. Eng.*, 2017, **5**, 6682–6691.
46 S. Gao, H. Fan and S. Zhang, *J. Mater. Chem. A*, 2014, **2**, 18263–18270.
47 Y. Liu, H. Jiang, Y. Zhu, X. Yang and C. Li, *J. Mater. Chem. A*, 2016, **4**, 1694–1701.
48 H. Zhao, T. Xing, L. Li, X. Geng, K. Guo, C. Sun, W. Zhou, H. Yang, R. Song and B. An, *Int. J. Hydrogen Energy*, 2019, **44**, 25180–25187.
49 Y. Huang, K. Ye, H. Li, W. Fan, F. Zhao, Y. Zhang and H. Ji, *Nano Res.*, 2016, **9**, 3881–3892.
50 C. Weng, J. Ren, Z. Hu and Z. Yuan, *ACS Sustainable Chem. Eng.*, 2018, **6**, 15811–15821.
51 J. Xia, N. Zhang, S. Chong, D. Li, Y. Chen and C. Sun, *Green Chem.*, 2018, **20**, 694–700.
52 C. Kim, C. Zhu, Y. Aoki and H. Habazaki, *Ind. Eng. Chem. Res.*, 2019, **58**, 3047–3059.
53 Y. Xing, Y. Wang, C. Zhou, S. Zhang and B. Fang, *ACS Appl. Mater. Interfaces*, 2014, **6**, 2561–2567.
54 D. Liu, X. Zhang, Y. Wang, S. Song, L. Cui, H. Fan, X. Qian and B. Fang, *Nanoscale*, 2020, **12**, 9524–9532.
55 Y. Xing, B. Fang, A. Bonakdarpour, S. Zhang and D. P. Wilkinson, *Int. J. Hydrogen Energy*, 2014, **39**, 7859–7867.
56 B. Fang, J. H. Kim, M.-S. Kim and J.-S. Yu, *Acc. Chem. Res.*, 2013, **46**, 1397–1406.
57 B. Fang, Y. Xing, A. Bonakdarpour, S. Zhang and D. P. Wilknson, *ACS Sustainable Chem. Eng.*, 2015, **3**, 2381–2388.
58 B. Fang, Y.-Z. Wei and M. Kumagai, *J. Power Sources*, 2006, **155**, 487–491.